Speckle reducing anisotropic diffusion for 3D ultrasound images

Qingling Sun[a], John A. Hossack[b,*], Jinshan Tang[c], Scott T. Acton[b,c]

[a]*Department of Computer Science, University of Virginia, Charlottesville, VA 22904-4743, USA*
[b]*Department of Biomedical Engineering, University of Virginia, Box 800759, Charlottesville, VA 22908, USA*
[c]*Department of Electrical and Computer Engineering, University of Virginia, Charlottesville, VA 22904-4743, USA*

Abstract

This paper presents an approach for reducing speckle in three dimensional (3D) ultrasound images. A 2D speckle reduction technique, speckle reducing anisotropic diffusion (SRAD), is explored and extended to 3D. 3D SRAD is advantageous in that, like 2D SRAD, it keeps the advantages of the conventional anisotropic diffusion and the traditional speckle reducing filter, the Lee filter, by exploiting the instantaneous coefficient of variation (ICOV). Besides, 3D SRAD uses 3D information; thus it overcomes the shortcoming of the 2D technique that only uses 2D information. The algorithm of 3D SRAD is presented in the continuous domain as well as in the discrete domain. Experiments have been performed on both synthetic and real 3D ultrasound images and the experimental results were compared with those obtained by 3D anisotropic diffusion and the 3D Lee filter. The experimental results show that the quality of the 3D SRAD for speckle reduction in 3D ultrasound images improves upon that of 3D anisotropic diffusion and 3D Lee filter in terms of edge preservation and the smoothness of homogenous regions.
© 2004 Elsevier Ltd. All rights reserved.

Keywords: Ultrasound imaging; 3D SRAD; Speckle reduction; Anisotropic diffusion

1. Introduction

Ultrasound imaging is popular and plays a unique role in clinical diagnosis and treatment because it is a non-invasive, non-radiative, real-time and inexpensive imaging modality [1,2]. There are two basic types of ultrasound imaging systems: 2D and 3D ultrasound imaging. The majority of current ultrasound imaging systems are two dimensional. However, conventional 2D ultrasound imaging has limitations in quantifying the volume of structures of interest in the body, for only a two dimensional frame is produced at any given time. In many cases volume quantification is important in assessing the progression of disease and tracking progression of response to treatment. Thus, 3D ultrasound imaging has drawn great attention in recent years [3–6].

To develop a more accurate approach for volume quantification, many approaches of 3D ultrasound image reconstruction have been developed. Current practice usually involves a 2D ultrasound machine and a position sensor attached to the ultrasound scanner probe. The 2D ultrasound machine provides slices of images through the structure of interest. The position sensor provides the relative position of these slices in space [7]. In the 'I-beam' method [8], shown in Fig. 1, a modified transducer provides the information needed to reconstruct the 3D image from a sequence of 2D slices captured by the modified linear 1D array at the center. The two perpendicular tracking arrays on each side of the central array provide the relative motion information between all the image slices, which is required when positioning and interpolating 2D slices in 3D volume [8]. However, the presence of speckle is a problem. Speckle in coherent imaging systems is the artifact caused by the interference of energy from randomly distributed scatterers [9]. In ultrasound imaging it is seen as a granular structure caused by the essentially random interaction of the multiple ultrasound waves scatterered from within the tissue [2].

---

* Corresponding author. Tel.: +1 434 243 5866; fax: +1 434 982 3870.
  E-mail addresses: qinglingsun@yahoo.com (Q. Sun), jh7fj@virginia.edu (J.A. Hossack), jt6w@virginia.edu (J. Tang), tangyiyong@yahoo.com (J. Tang), acton@virginia.edu (S.T. Acton).
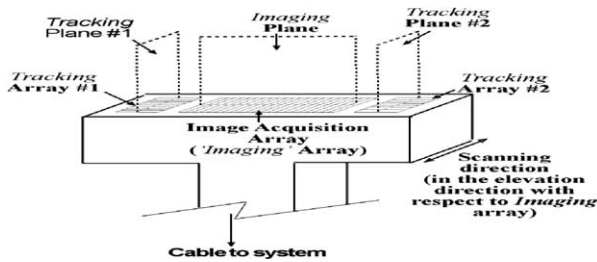
Fig. 1. I-beam transducer [8].

Fig. 2. Basic steps of the procedure of 3D volume measurement.

Speckle degrades both the spatial resolution and contrast quality in ultrasound images [5] and therefore makes the interpretation of ultrasound image more difficult. Additionally, it makes image segmentation difficult.

Speckle is not an additive noise, but rather a form of multiplicative noise [10–15]. Noise reduction filters such as conventional anisotropic diffusion and the Lee filter are not effective for the purpose of speckle reduction. The conventional anisotropic diffusion is effective for additive noise, but not for multiplicative noise—including speckle. The traditional speckle removal filters, such as the Lee filter [14] and Frost filter [15] have major limitations in edge preserving and feature preserving [12]. Thus, by combining the advantages of the above two filters by exploiting the instantaneous coefficient of variation, 2D SRAD was developed [12,13]. Compared with the existing noise reducing schemes, the results indicate that 2D SRAD excels in terms of mean preservation, variance reduction and edge localization in the presence of speckle noise [12].

3D SRAD is developed in this paper. 3D SRAD operates directly on image volume instead of the 2D slice. Thus, information between slices of 2D image are explored and preserved.

The rest of this paper is organized as follows: in Section 2, some background information on cardiovascular research and 2D SRAD are introduced. Section 3 provides some improvement of the 2D SRAD algorithm and Section 4 presents the algorithms for speckle reduction in 3D ultrasound images. Three 3D filters (3D Anisotropic diffusion, 3D SRAD and 3D Lee filter) for speckle reduction in 3D ultrasound images are derived. Experimental results and conclusion are presented in Sections 5 and 6, respectively.

2. Background

2.1. Three dimensional ultrasound imaging

In this section some background knowledge of quantitative ultrasound imaging of mouse hearts and the importance of applying 3D SRAD in 3D ultrasound imaging are introduced.

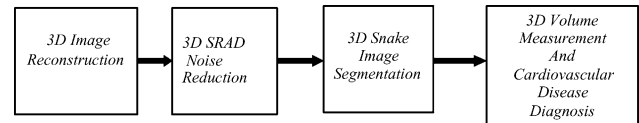The aim of quantitative ultrasound imaging of mouse hearts is to provide an effective high frequency quantitative imaging technique for research related to human cardiovascular disease which is the leading cause of death in the United States. Heart failure frequently evolves in a structured manner following a myocardial infarction (MI). Left ventricular remodeling (LVR) is usually involved following a significant anterior MI. However, excessive LVR might cause increased left ventricular (LV) end-systolic volume that is the main cause for patient mortality after recovery from MI. To track the subsequent recovery following MI, a non-invasive image tracking method is needed for the study of heart anatomy and function. Due to the features mentioned earlier, ultrasound imaging is more advantageous than other tracking approaches such as histology and MR imaging for this purpose [16,17].

To fulfill this task, an ultrasound transducer that is compatible with high spatial resolution and 3D image reconstruction is required. This transducer should be capable of a spatial resolution of 200 μm laterally and 100 μm axially with a frame rate of 100+ frames per second. Also, this transducer should be able to provide the information for the 3D position and orientation [11]. The I-beam [8] method suits this purpose. After the 3D reconstruction, image segmentation technique will be used to automatically determine the endocardial and epicardial surface. This enables a variety of significant cardiac parameters to be calculated, including: end-systole LV volume, end-diastole (ED) LV volume, LV ejection fraction (EF), LV mass and cardiac output (CO) [11]. However, speckle artifacts, unavoidable in coherent wave based ultrasound imaging, make image segmentation difficult. Thus, speckle reduction becomes a necessary preconditioning step prior to image segmentation and volume quantification. The basic steps needed in the procedure of the volume quantification are shown in Fig. 2. Among these steps, step two is of our interest in this paper. Fig. 3 shows a reconstructed 3D left ventricular of mouse heart.
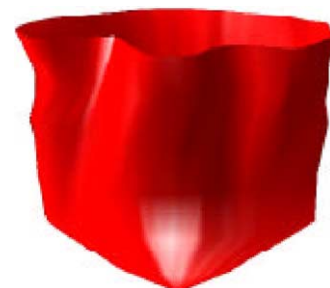

Fig. 3. 3D mouse LV reconstruction (scale: about 5 mm in each dimension).

2.2. An existing effective algorithm for speckle reduction—2D SRAD

The features of the speckle make the conventional noise reduction filters such as anisotropic diffusion and the Lee filter ineffective. 2D SRAD, a diffusion method tailored to speckle reduction in ultrasound and radar image, was derived. Combining the advantages of the conventional anisotropic diffusion and the Lee filter, 2D SRAD inherits the partial differential equation format of the conventional anisotropic diffusion and exploits the instantaneous coefficient of variation (ICOV) in the same way as the Lee filter utilizes the coefficient of variation in adaptive filtering [12,13]. On the other hand, 2D SRAD overcomes the shortcomings of these two filters.

2D SRAD is based on traditional anisotropic diffusion, which is a nonlinear filtering method that encourages diffusion in the homogeneous region while inhibits diffusion at edges. The PDE of anisotropic diffusion is given as follows in continuous domain [12,13]

$$\begin{cases} \dfrac{\partial I}{\partial t} = \mathrm{div}[c(|\nabla I|)\nabla I] \\ I(t = 0) = I_0 \end{cases} \tag{1}$$

where ∇ is the gradient operator, div is the divergence operator, $\|$ denotes the magnitude, $c(x)$ is the diffusion coefficient, and I_0 is the initial image.

2D SRAD takes the format of the PDE of conventional anisotropic diffusion. Given an intensity image $I_0(x, y)$ having none zero-valued intensities over the image domain Ω, the continuous form of SRAD is expressed as follows [12]

$$\begin{cases} \partial I(x, y; t)/\partial t = \mathrm{div}[c(x, y; t)\nabla I(x, y; t)] \\ I(x, y; 0) = I_0(x, y), (\partial I(x, y; t)/\partial \vec{n})|\partial \Omega = 0 \end{cases} \tag{2}$$

where $\partial \Omega$ denotes the border of Ω, $\vec{n}$ is the outer normal to the $\partial \Omega$, $c(x)$ is the diffusion coefficient, and q is the ICOV.

Observing Eqs. (1) and (2), we can see that the main difference between the two PDEs lie in the choice of diffusion coefficient $c(x)$. In conventional anisotropic diffusion, the diffusion coefficient is given by

$$c_d(x, y) = \exp\left(-\left[\frac{\nabla I_d(x, y)}{k}\right]^2\right) \tag{3}$$

where $\nabla I_d(x, y)$ is the directional derivative in direction d at location (x, y). While in 2D SRAD the diffusion coefficient is a function of q, the instantaneous coefficient of variation [12]:

$$c(x, y, t) = \frac{1}{1 + [q^2(x, y; t) - q_0^2(t)]/[q_0^2(t)(1 + q_0^2(t))]} \tag{4}$$

where $q(x, y; t)$ is given by

$$q(x, y; t) = \sqrt{\frac{|(1/2)(|\nabla I|/I)^2 - (1/4^2)(\nabla^2 I/I)^2|}{[1 + (1/4)(\nabla^2 I/I)]^2}}, \tag{5}$$

and q_0, the speckle scale computed from a homogenous region, can be computed by

$$q_0(t) = \frac{\sqrt{\mathrm{var}[z(t)]}}{\bar{z(t)}} \tag{6}$$

From Eqs. (2), (4) and (5), we can see that when q is smaller, c will be larger, thus diffusion will be encouraged in homogeneous region and inhibited at edges in 2D SRAD. This is in accordance with the conventional anisotropic diffusion, which does smoothing, where the local gradient magnitude is low and inhibit diffusion, where the gradient magnitude is relatively high.

Another filter relevant to 2D SRAD is the Lee filter. The importance of the Lee filter to 2D SRAD lies in providing prototype of coefficient of variation for q and q_0.

The Lee filter, an adaptive speckle filter, was designed to remove speckle in radar image. The equation is given as follows [14]

$$\hat{I}_s = \bar{I}_s + k_s(I_s - \bar{I}_s) \tag{7}$$

where $\bar{I}_s$ is the mean value of the intensity within the filter window η_s; and k_s is the adaptive filter coefficient determined by

$$k_s = 1 - C_u^2/C_s^2. \tag{8}$$

where

$$C_s^2 = (1/|\eta_s|)\sum_{p\in\eta}(I_p - \bar{I}_s)^2/(\bar{I}_s)^2, \tag{9}$$

and C_u^2 is a constant for a given image and can be determined by

$$C_u^2 = \frac{\mathrm{var}(z')}{(\bar{z}')^2} \tag{10}$$

where $\mathrm{var}(z')$ and $\bar{z}'$ are the intensity variance and mean over a homogeneous area of the image, respectively.

Comparing Eqs. (5) and (6) with Eqs. (9) and (10), we can see that the speckle scale function of 2D SRAD (see Eq. (6)) directly takes the format of the coefficient of variation function of Lee filter (see Eq. (10)). Besides, the ICOV function defined in Eq. (5) is derived from Eq. (9) in the Lee filter [12,13].

3. Analysis and improvement of SRAD algorithm

One of the key steps in the SRAD algorithm is to choose a homogenous region to compute q_0. The choice of this region will affect the diffusion results dramatically.

In order to develop a stable computation of $q_0(t)$, let's analyze the performance of the SRAD algorithm. Let

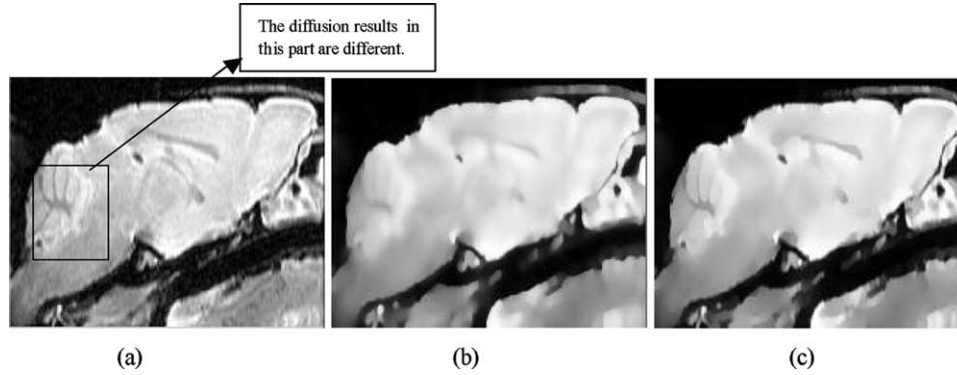$$P(x, y; t) = (q^2(x, y; t) - q_0^2(t))/q_0^2(t) \tag{11}$$

Fig. 4. Comparison between original SRAD algorithm and improved SRAD algorithm; (a) original image [22] used to make an image with multiplicative noise by exponential operation; (b) original SRAD algorithm; (c) Improved SRAD algorithm ($\lambda = 1.1$).

and

$$Q(t) = 1 + q_0^2(t) \tag{12}$$

thus $c(x, y; t)$ can be expressed as

$$c(x, y; t) = \frac{1}{1 + P(x, y; t)/Q(t)} \tag{13}$$

$P(x; y; t)$ is the main part which affects the diffusion, and $Q(t)$ is used to normalize $P(x, y; t)$ such that $P(x, y; t)$ lies in the range $(-1, 1)$. When $q^2(x, y; t) = q_0^2(t)$, $c(x, y; t)$ is 1; when $q^2(x, y; t) > q_0^2(t)$, $c(x, y; t) < 1$; when $q^2(x, y; t) < q_0^2(t)$, $c(x, y; t) > 1$. Thus, if we assume that $c(x, y; t)$ is the speed of diffusion, then the diffusion will progress in different speeds in different regions, which is a little different from conventional anisotropic diffusion processing: in the region similar to the selected homogenous region with $q^2(x, y; t) \approx q_0^2(t)$, the diffusion speed is moderate; in the region smoother than the selected homogenous region with $q^2(x, y; t) < q_0^2(t)$, the diffusion is faster; In the region with $q^2(x, y; t) > q_0^2(t)$, the diffusion is slower. Thus, $q_0^2(t)$ provides a reference point for diffusion. In fact, if $q_0^2(t)$ is computed using the most smooth region (assume that all $q^2(x, y; t)$ is more than $q_0^2(t)$), the diffusion processing will degrade into conventional anisotropic diffusion: in the region similar to the selected homogenous region with $q^2(x, y; t) \approx q_0^2(t)$, the diffusion will be encouraged, and diffusion will be inhibited, where gradient magnitude is relatively high (with $q^2(x, y; t) > q_0^2(t)$).

Now that $q_0(t)$ provides a reference point for diffusion, we can use other technique to obtain it independent of selecting a region to compute it. One way to replace q_0 is to use the mean of $q(x, y; t)$, such that $c(x, y; t)$ is modified as

$$c(x, y; t) = \frac{1}{1 + [q^2(x, y; t) - q_0^2(t)]/[q_0^2(t)(1 + q_0^2(t))]} \tag{14}$$

where

$$q_0(t) = \lambda \iint_A q^2(x, y; t) \mathrm{d}x\,\mathrm{d}y / \iint_A \mathrm{d}x\,\mathrm{d}y \tag{15}$$

where A is the image domain and λ is a parameter that can be used to control the diffusion results. If we prefer to preserve edges, we can realize it by selecting a suitable λ. Eq. (14) allows the diffusion to progress as follows: in the region with contrast larger than the average contrast, the diffusion speed is slower; in the region with contrast smaller than the average contrast, the diffusion is faster; in the region with contrast similar to the average contrast, the diffusion is moderate. Fig. 4(c) shows the diffusion results using Eq. (14). From Fig. 4(c), the edge preservation of the resultant image obtained by the new algorithm is better than that obtained by the original SRAD algorithm. In Fig. 4, the image in Fig. 4(a) is the original image [22] with multiplicative noise used as the input to the SRAD algorithm.

4. Speckle reduction for 3D ultrasound images

As we have described in introduction, with the development of 3D ultrasound imaging systems, we need to develop techniques to perform speckle reduction for 3D ultrasound images. One way to perform speckle reduction for 3D US images is to perform speckle reduction for each 2D slice, which is from the 3D images, using 2D speckle reduction technique described in Section 2. Fig. 5 shows a result of speckle reduction of 3D images using 2D SRAD. From Fig. 5, we can find that the speckle reduction results are not acceptable in that there are obvious block effects. The reason is that this simple technique just uses 2D information instead of 3D information. In order to develop an effective speckle reduction technique for 3D US images, we extend 2D SRAD to 3D algorithm.

4.1. 3D anisotropic diffusion

The PDE of 3D anisotropic diffusion takes the similar form as 2D anisotropic diffusion

$$\frac{\partial I(x, y, z; t)}{\partial t} = \mathrm{div}[c(x, y, z; t)\nabla I(x, y, z; t)] \tag{16}$$
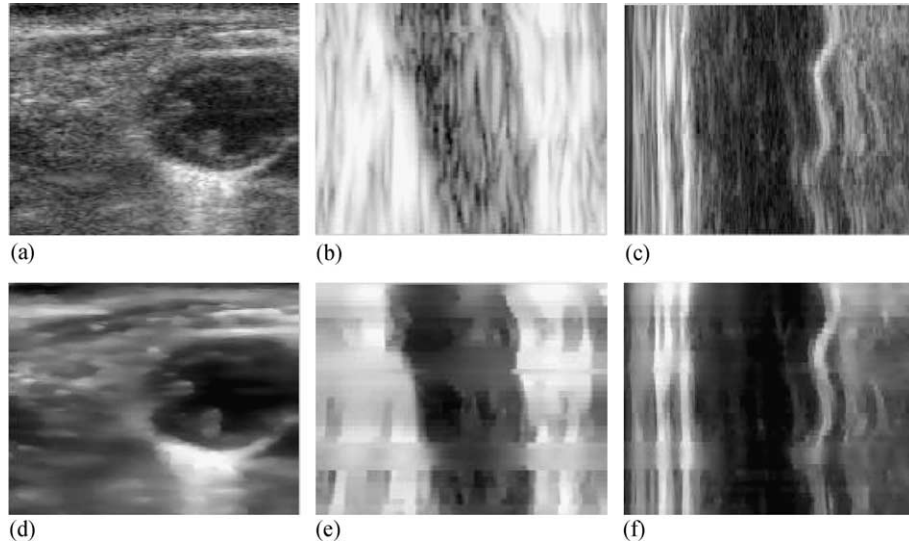
Fig. 5. Speckle reduction using the improved 2D SRAD algorithm for a 3D US image; (a)–(c) are the original images arbitrarily sliced out from the speckled experimental image volume along *XY*-, *XZ*-, *YZ*-planes, respectively. (d)–(f) are resultant images after diffusion corresponding to (a)–(c).

Eq. (16) is equivalent to

$$\frac{\partial I(x,y,z;t)}{\partial t} = \text{div}[c(x,y,z;t)\nabla I(x,y,z;t)]$$

$$= \frac{\partial}{\partial x}\left(c(x,y,z;t)\times\frac{\partial}{\partial x}I(x,y,z;t)\right)$$

$$+ \frac{\partial}{\partial y}\left(c(x,y,z;t)\times\frac{\partial}{\partial y}I(x,y,z;t)\right)$$

$$+ \frac{\partial}{\partial z}\left(c(x,y,z;t)\times\frac{\partial}{\partial z}I(x,y,z;t)\right) \quad (17)$$

The above equation can be implemented using a finite difference method. Consider the difference approximation of

$$\frac{\partial}{\partial x}\left(c(x,y,z;t)\times\frac{\partial}{\partial x}I(x,y,z;t)\right)$$

which is expressed as

$$\frac{\partial}{\partial x}\left(c(x,y,z;t)\times\frac{\partial}{\partial x}I(x,y,z;t)\right)$$

$$\approx \frac{\partial}{\partial x}\left\{c(x,y,z;t)\frac{1}{\Delta x}[I(x+\Delta x,y,z;t) - I(x,y,z;t)]\right\}$$

$$\approx \frac{1}{\Delta x^2}\{c(x,y,z;t)[I(x+\Delta x,y,z;t) - I(x,y,z;t)$$

$$- I(x,y,z;t) + I(x-\Delta x,y,z;t)]$$

$$+ [c(x+\Delta x,y,z;t) - c(x,y,z;t)][I(x+\Delta x,y,z;t)$$

$$- I(x,y,z;t)]\}$$

$$= \frac{1}{\Delta x^2}\{c(x+\Delta x,y,z;t)[I(x+\Delta x,y,z;t)$$

$$- I(x,y,z;t)] + c(x,y,z;t)[I(x-\Delta x,y,z;t)$$

$$- I(x,y,z;t)]\} \quad (18)$$

$$= \frac{1}{\Delta x^2}\{c(x+\Delta x,y,z;t)[I(x+\Delta x,y,z;t) - I(x,y,z;t)]$$

$$+ c(x,y,z;t)[I(x-\Delta x,y,z;t) - I(x,y,z;t)]\}$$

where '$\approx$' means that the right of the equation is the difference approximation of the left of the equation. Similarly, we have

$$\frac{\partial}{\partial y}\left(c(x,y,z;t)\times\frac{\partial}{\partial y}I(x,y,z;t)\right) \approx \frac{1}{\Delta y^2}\{c(x,y+\Delta y,z;t)$$

$$\times[I(x,y+\Delta y,z;t) - I(x,y,z;t)] + c(x,y,z;t)$$

$$\times[I(x,y-\Delta y,z;t) - I(x,y,z;t)]\} \quad (19)$$

$$\frac{\partial}{\partial z}\left(c(x,y,z;t)\times\frac{\partial}{\partial z}I(x,y,z;t)\right) \approx \frac{1}{\Delta z^2}\{c(x,y,z+\Delta z;t)$$

$$\times[I(x,y,z+\Delta z;t) - I(x,y,z;t)] + c(x,y,z;t)$$

$$\times[I(x,y,z-\Delta z;t) - I(x,y,z;t)]\} \quad (20)$$

Inserting Eqs. (18)–(20) into (17) and letting $\Delta x=1$, $\Delta y=1$, $\Delta z=1$, we obtain the difference approximation of

$\delta I(x,\ y,\ z;\ t)/\delta t$ which is expressed as

$$
\begin{aligned}
\frac{\partial I(x,y,z;t)}{\partial t} \approx\ & c(x+1,y,z;t)[I(x+1,y,z;t)-I(x,y,z;t)] \\
& + c(x,y,z;t)[I(x-1,y,z;t)-I(x,y,z;t)] \\
& + c(x,y+1,z;t)[I(x,y+1,z;t)-I(x,y,z;t)] \\
& + c(x,y,z;t)[I(x,y-1,z;t)-I(x,y,z;t)] \\
& + c(x,y,z+1;t)[I(x,y,z+1;t)-I(x,y,z;t)] \\
& + c(x,y,z;t)[I(x,y,z-1;t)-I(x,y,z;t)].
\end{aligned}
\tag{21}
$$

Thus, the discrete realization of anisotropic diffusion for 3D image can be obtained from Eq. (21) as follows

$$
\begin{aligned}
I(x,y,z;t+1) =\ & I(x,y,z;t) + c(x+1,y,z;t)[I(x+1,y,z;t) \\
& - I(x,y,z;t)] \\
& + c(x,y,z;t)[I(x-1,y,z;t)-I(x,y,z;t)] \\
& + c(x,y+1,z;t)[I(x,y+1,z;t)-I(x,y,z;t)] \\
& + c(x,y,z;t)[I(x,y-1,z;t)-I(x,y,z;t)] \\
& + c(x,y,z+1;t)[I(x,y,z+1;t)-I(x,y,z;t)] \\
& + c(x,y,z;t)[I(x,y,z-1;t)-I(x,y,z;t)].
\end{aligned}
\tag{22}
$$

From Eq. (22), we can find that the key problem in anisotropic diffusion is the choice of $c(x, y, z; t)$. Similar to 2D anisotropic diffusion, $c(x, y, z; t)$ can be chosen as follows:

$$
c(x,y,z;t) = \exp\left(-\left[\frac{\nabla I(x,y,z;t)}{k}\right]^2\right),
\tag{23}
$$

or

$$
c(x,y,z;t) = \frac{1}{1 + \left[\frac{\nabla I(x,y,z;t)}{k}\right]^2}.
\tag{24}
$$

4.2. 3D SRAD Algorithm

From Yu and Acton's work on 2D SRAD [12], we know that the traditional anisotropic diffusion is not suitable for speckle reduction in 2D US image, thus an improved version of anisotropic diffusion using ICOV was developed. Similarly, for 3D US images, the 3D anisotropic diffusion filter Eqs. (16)–(18) is also not suitable for speckle reduction in 3D US image (see Section 5). Thus we developed 3D SRAD algorithm for 3D US images.

4.2.1. 3D SRAD algorithm in continuous domain

3D SRAD algorithm is derived from 2D SRAD algorithm. Similar to 2D SRAD, the continuous form of 3D SRAD can be obtained using 3D image $I(x, y, z; t)$ to

replace two dimensional image $I(x, y; t)$ in (2)

$$
\begin{cases}
\partial I(x,y,z;t)/\partial t = \mathrm{div}[c(q)\nabla I(x,y,z;t)] \\
I(x,y,z;0) = I_0(x,y,z), (\partial I(x,y,z;t)/\partial \vec{n})|\partial \Omega = 0
\end{cases}
\tag{25}
$$

where $\partial \Omega$ denotes the border of Ω, $\vec{n}$ is the outer normal to the $\partial \Omega$ and the diffusion coefficient $c(q)$ is given by

$$
c(q) = \frac{1}{1 + [q^2(x,y,z;t) - q_0^2(t)]/[q_0^2(t)(1 + q_0^2(t))]}
\tag{26}
$$

where $q(x, y, z; t)$ is called 3D instantaneous coefficient of variation which can be derived in the same way to obtain the instantaneous coefficient of variation in 2D SRAD [21]

$$
q(x,y,z,t) = \sqrt{\frac{(1/3)(|\nabla^2 I|/I)^2 - (1/6)^2(\nabla^2 I/I)^2}{(1 + (1/6)(\nabla^2 I/I))^2}}
\tag{27}
$$

Let's consider how to obtain the 3D instantaneous coefficient of variation. Modifying Eq. (25) in [12] into Eq. (28)

$$
C_{i,j,k}^2 = \frac{\left[I_{i,j,k}^2 + \frac{1}{|\bar{\eta}_s|}\nabla^2 I_{i,j,k}^2\right]}{\left[I_{i,j,k} + \frac{1}{|\bar{\eta}_s|}\nabla^2 I_{i,j,k}\right]^2} - 1.
\tag{28}
$$

In the continuous domain, we have [12]

$$
\nabla^2 I^2 = 2|\nabla I|^2 + 2I\nabla^2 I
\tag{29}
$$

In the discrete domain, (29) can be represented as follows

$$
\nabla^2 I_{i,j,k}^2 = |\nabla_1 I_{i,j,k}|^2 + |\nabla_2 I_{i,j,k}|^2 + 2I_{i,j,k}\nabla^2 I_{i,j,k}.
\tag{30}
$$

where $\nabla_1 I_{i,j,k}$ and $\nabla_2 I_{i,j,k}$ are obtained by

$$
\nabla_1 I_{i,j,k} = [I_{i,j,k} - I_{i-1,j,k}, I_{i,j,k} - I_{i,j-1,k}, I_{i,j,k} - I_{i,j,k-1}]
\tag{31}
$$

$$
\nabla_2 I_{i,j,k} = [I_{i+1,j,k} - I_{i,j,k}, I_{i,j+1,k} - I_{i,j,k}, I_{i,j,k+1} - I_{i,j,k}].
\tag{32}
$$

Let $|\nabla I_{i,j,k}|^2$ be discretized as the average of $|\nabla_1 I_{i,j,k}|^2$ and $|\nabla_2 I_{i,j,k}|^2$, and substituting Eqs. (31) and (32) into Eq. (28), then we have [21]

$$
C_{i,j,k}^2 = \frac{\frac{1}{3}|\nabla I_{i,j,k}|^2 - \frac{1}{36}(\nabla^2 I_{i,j,k})^2}{\left[I_{i,j,k} + \frac{1}{6}\nabla^2 I_{i,j,k}\right]^2}.
\tag{33}
$$

Denoting the special case of $C_{i,j,k}$, which is computed over $\bar{\eta}_s$, by $q_{i,j}$, then $q_{i,j}$ can be viewed as a discretization of

$$
q = \sqrt{\frac{(1/3)(|\nabla I|/I)^2 - (1/6)^2(\nabla^2 I/I)^2}{(1 + (1/6)(\nabla^2 I/I))^2}}.
\tag{34}
$$

4.2.2. Numerical implementation of 3D SRAD algorithm

Eq. (25) can be solved numerically using four-stage iterative method [12]. Let the time step be Δt and the spatial step be h in x, y and z directions, then the time and space coordinates can be discretized as: $t = n\Delta t$, $n = 0,1,2,\ldots$; $x = ih$, $y = jh$, $z = kh$; $i = 0,1,2,\ldots M-1$, $j = 0,1,2,\ldots N-1$, $k = 0,1,2,\ldots K-1$, where $Mh \times Nh \times Kh$

is the size of the image support. Let $I_{i,j,k}^n = I(ih, jh, kh, n\,\Delta t)$, then the three stages can be described as:

Stage 1. Computing the derivative approximations and the Laplacian approximation

$$\nabla_1 I_{i,j,k}^n = \left[\frac{I_{i+1,j,k}^n - I_{i,j,k}^n}{h}, \frac{I_{i,j+1,k}^n - I_{i,j,k}^n}{h}, \frac{I_{i,j,k+1}^n - I_{i,j,k}^n}{h} \right],$$

(35)

$$\nabla_2 I_{i,j,k}^n = \left[\frac{I_{i,j,k}^n - I_{i-1,j,k}^n}{h}, \frac{I_{i,j,k}^n - I_{i,j-1,k}^n}{h}, \frac{I_{i,j,k}^n - I_{i,j,k-1}^n}{h} \right],$$

(36)

$$\nabla^2 I_{i,j,k}^n$$

$$= \frac{I_{i+1,j,k}^n + I_{i-1,j,k}^n + I_{i,j+1,k}^n + I_{i,j-1,k}^n + I_{i,j,k+1}^n + I_{i,j,k-1}^n - 6I_{i,j,k}^n}{h^2}.$$

(37)

The symmetric boundary conditions are used

$$I_{-1,j,k}^n = I_{0,j,k}^n, \quad I_{M,j,k}^n = I_{M-1,j,k}^n, \quad j = 0,1,2,\ldots,N-1,$$

$$k = 0,1,2,\ldots,K-1.$$

(38)

$$I_{i,-1,k}^n = I_{i,0,k}^n, \quad I_{i,N,k}^n = I_{i,N-1,k}^n, \quad i = 0,1,2,\ldots,M-1,$$

$$k = 0,1,2,\ldots,K-1.$$

(39)

$$I_{i,j,-1}^n = I_{i,j,0}^n, \quad I_{i,j,K}^n = I_{i,j,K-1}^n, \quad i = 0,1,2,\ldots,M-1,$$

$$j = 0,1,2,\ldots,N-1.$$

(40)

Stage 2. Computing the diffusion coefficient $c(q)$

$$c_{i,j}^n = c\left[q\left(\frac{1}{I_{i,j,k}^n} \sqrt{|\nabla_1 I_{i,j,k}^n|^2 + |\nabla_2 I_{i,j,k}^n|^2}, \frac{1}{I_{i,j,k}^n} \nabla^2 I_{i,j,k}^n \right) \right].$$

(41)

Stage 3. Computing the divergence of $c(\cdot)\nabla I$

$$d_{i,j,k}^n = \frac{1}{h^2}[c_{i+1,j,k}^n(I_{i+1,j,k}^n - I_{i,j,k}^n) + c_{i,j,k}^n(I_{i-1,j,k}^n - I_{i,j,k}^n)$$

$$+ c_{i,j+1,k}^n(I_{i,j+1,k}^n - I_{i,j,k}^n)] + \frac{1}{h^2}[c_{i,j,k}^n(I_{i,j-1,k}^n - I_{i,j,k}^n)$$

$$+ c_{i,j,k+1}^n(I_{i,j,k+1}^n - I_{i,j,k}^n) + c_{i,j,k}^n(I_{i,j,k-1}^n - I_{i,j,k}^n)]$$

(42)

with symmetric boundary conditions:

$$d_{-1,j,k}^n = d_{0,j,k}^n, \quad d_{M,j,k}^n = d_{M-1,j,k}^n, \quad j = 0,1,2,\ldots,N-1,$$

$$k = 0,1,2,\ldots,K-1.$$

(43)

$$d_{i,-1,k}^n = d_{i,0,k}^n, \quad d_{i,N,k}^n = d_{i,N-1,k}^n, \quad i = 0,1,2,\ldots,M-1,$$

$$k = 0,1,2,\ldots,K-1.$$

(44)

$$d_{i,j,-1}^n = d_{i,j,0}^n, \quad d_{i,j,K}^n = d_{i,j,K-1}^n, \quad i = 0,1,2,\ldots,M-1,$$

$$j = 0,1,2,\ldots,N-1.$$

(45)

Stage 4. The numerical approximation to the differential equation is given by

$$I_{i,j}^{n+1} = I_{i,j}^n + \frac{\Delta t}{6} d_{i,j}^n.$$

(46)

Similar to [12], (46) is also called the *SRAD update function* for 3D SRAD. In numerical implementation, h is set to 1, and empirically Δt is set to 0.05.

4.3. 3D Lee filter

For comparison, we also developed a 3D Lee filter. The 3D Lee filter has the same form the 2D Lee filter in (7)–(10), with the only difference lying in that we will use the 3D image $I(x, y, z)$ instead of the 2D image $I(x, y)$.

5. Experimental results

5.1. Images

3D synthetic radio frequency (rf) ultrasound images generated using the method in [18] and real 3D ultrasound images obtained by I-beam are used in the experiments. The reason for using synthetic images is the need for quantitative analysis. Three 3D synthetic images and five 3D US images were used in the experiments. The size of the synthetic rf images is $512 \times 128 \times 50$ (in units of pixels) in x, y and z directions, respectively. The size of the real 3D ultrasound images image is $473 \times 149 \times 41$ (in units of pixels) in x, y and z directions, respectively.

5.2. Performance metrics

Two performance metrics were used in our experiments to measure the algorithm performance, one is called contrast measure which is used to measure the performance in the homogenous region. The other measure is the Pratt's figure of merit [19], which is used to measure the edge preservation.

5.2.1. Contrast measure

The metric is based on a local contrast measure. Let $I(x, y, z)$ be the pixel value at the coordinates (x, y, z) and its $2n+1$ neighborhood, then the local contrast at the pixel (x, y, z) is defined as

$$C(x, y, z) = \frac{I_{\max}(x, y, z) - I_{\min}(x, y, z)}{I_{\max}(x, y, z) + I_{\min}(x, y, z)}$$

(47)

where $I_{\max}(x, y, z)$ and $I_{\min}(x, y, z)$ are the maximum and minimum values of the pixels in its $2n+1$ neighborhood, respectively.

The metric used to measure performance of the diffusion algorithm in a region can be represented by the average contrast in that region, which is defined as

$$C = \frac{\sum_{(x,y,z)\in\Omega} C(x,y,x)}{N} \qquad (48)$$

where Ω is an image region and N is pixel number in the region. A good diffusion algorithm should produce the following effect: the homogenous region in the image after diffusion should have much less contrast than that in the homogenous region in the image before diffusion.

5.2.2. Pratt's quality measurement [12,19]

The performance used for measuring the performance of edge preservation is Pratt's quality measurement. The metric can be expressed as [19]

$$FOM = \frac{\sum_{i=1}^{I_A} \dfrac{1}{1 + \alpha(d(i)^2)}}{\max(I_A, I_I)} \qquad (49)$$

where I_A is the number of edge pixels detected and I_I is the number of ideal pixels. $d(i)$ is the Euclidean distance between the ith detected pixel and the nearest ideal pixel. α is a scaling constant, with a suggested value of 1/9 [19]. In the experiments, a 3D edge detection technique based on [20] is used to detect the edges in the images.

5.3. Results

Sections 5.3.1 and 5.3.2 provides comparison results: one is the comparison results among the 3D filters, the other is the comparison results between the 2D SRAD algorithm and the 3D SRAD algorithm.

5.3.1. Results for 3D synthetic radio frequency (rf) ultrasound images

We first present the experimental results using the three 3D synthetic radio frequency ultrasound images. Fig. 6(a), (c) and (e) are the original speckled rf images arbitrarily sliced out from the speckled rf image volume along *XY*-, *XZ*-, *YZ*-planes, respectively and Fig. 6(b), (d) and (f) are the resultant images after diffusion corresponding to Fig. 6(a), (c) and (e). By comparing the original images (a), (c) and (e) with the corresponding resultant images in each figure, we can observe qualitatively that the speckle is effectively removed after the 3D SRAD is applied. Table 1 summarizes the performance of diffusion in two different regions: one is the region composed of the boundary pixels of the ball, the other region is composed of all the pixels except the pixels from the ball boundary. The locations of the pixels in the boundary are marked before we put the speckles into the original image. Tables 1 and 2 clearly show that the 3D SRAD improves upon the performance of 3D Lee filter, traditional anisotropic diffusion and the 2D SRAD in contrast reduction in the homogeneous region and in the preservation of edges.
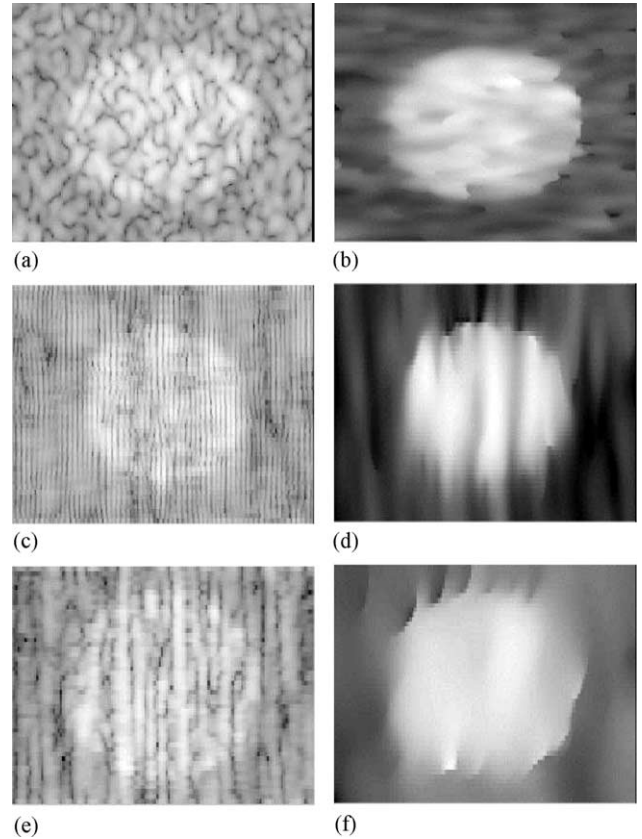

Fig. 6. Experimental results obtained by 3D anisotropic diffusion; (a), (c) and (e) are the original speckled rf images arbitrarily sliced out from the speckled rf image volume along *XY*-, *XZ*-, *YZ*-planes, respectively. (b), (d) and (f) Resultant images after diffusion corresponding to (a), (c) and (e).

5.3.2. Results for real ultrasound images

The second experiment uses real ultrasound image obtained using the prototype I-beam transducer. Five 3D ultrasound images were used in the experiments. The resultant images are compared to original images and displayed in 2D. Resultant images displayed in 2D are obtained by arbitrarily slicing from the 3D resultant image. Fig. 7(a)–(c) are the original images arbitrarily sliced out from a 3D speckled real ultrasound image volume along *XY*-,

Table 1

Contrast measured in homogenous region using 3D synthetic radio frequency ultrasound images

Image no.	Original	AD	3D SRAD	2D SRAD	Lee filter
1	0.5452	0.0231	0.0012	0.2573	0.1892
2	0.5070	0.0236	0.0056	0.3687	0.1743
3	0.6123	0.0235	0.0040	0.3895	0.0805

Table 2

FOM measured for 3D synthetic radio frequency ultrasound images

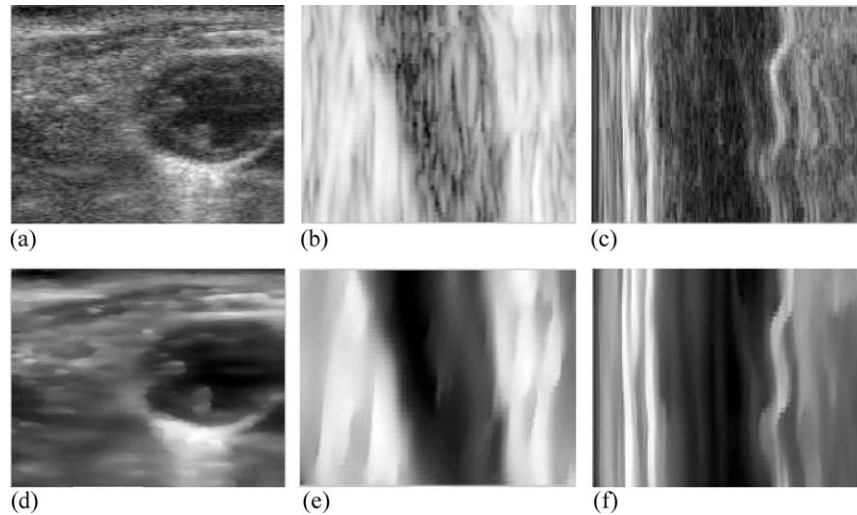| Image no.	Original	AD	3D SRAD	2D SRAD	Lee filter
1	0.0969	0.4423	0.6937	0.332	0.3826
2	0.0981	0.1814	0.5159	0.1057	0.1214
3	0.0929	0.1723	0.6021	0.1643	0.1525

Fig. 7. (a)–(c) are the original images arbitrarily sliced out from the speckled experimental image volume along *XY*-, *XZ*-, *YZ*-planes, respectively. (d)–(f) Resultant images after diffusion corresponding to (a)–(c) using 3D SRAD.

XZ-, *YZ*-planes, respectively and Fig. 7(d)–(f) are the resultant images after diffusion corresponding to Fig. 7(a)–(c). From Fig. 7, we observe that the diffusion results are good. It reduced the speckles but preserved the edge of the image. Besides visual checking, we also performed the quantitative analysis. In order to perform quantitative analysis, for each 3D image, we used three 2D images sliced from it. The 2D images sliced from the 3D images are the 2D images sliced along *XY*-, *XZ*-, *YZ*-planes, respectively. We compared the diffusion effect in the homogenous region before and after the diffusion. From each 2D image, we chose the region which is the mouse heart as the homogenous region and computed the contrast before and after the diffusion. For each 3D image, the contrast is the average of the contrasts of its three 2D images sliced out from it. Table 3 lists performance measured used the metric in Eq. (48). From Table 3, we have clearly found that the 3D SRAD performs better than Lee filter, AD filter and 2D SRAD.

We have implemented our algorithm using Matlab on a 1.5 GHz Pentium 4. For the 3D real ultrasound data set, the entire computation time was about 25 minutes. We anticipate that the speed can be made at least 10 times faster by modifying the Matlab code to C/C++ code. As the technique is parallelizable, opportunities for further improvement in computational expense exist via multi-processor implementation on a architecture such as the Mercury Adapdev.

6. Conclusion

In this paper 2D speckle reducing anisotropic diffusion, which is effective for speckle reduction in 2D ultrasound image is explored and extended into 3D. This development has significance for several ultrasound imaging projects in the area of cardiovascular disease diagnosis and cancer detection, such as the quantitative ultrasound imaging of mouse heart, high resolution 3D transrectal ultrasound, etc. The importance of 3D SRAD lies in its role as the preconditioning step prior to the image segmentation, which in turn is the preconditioning step prior to the volume quantification. Experiment results on synthetic radio frequency ultrasound image and experimental ultrasound image proved the effectiveness of 3D SRAD algorithm.

Table 3
CONTRAST measured in homogenous region for real ultrasound images obtained by I-beam

Image no.	Original	AD	3D SRAD	2D SRAD	Lee filter
1	0.2911	0.1821	0.0913	0.2561	0.2046
2	0.3112	0.1918	0.0824	0.2761	0.2134
3	0.3032	0.1631	0.1456	0.2675	0.1821
4	0.2941	0.1023	0.1077	0.2516	0.2133
5	0.4636	0.1215	0.0645	0.33	0.2301

References

[1] http://www.cs.uwa.edu.au/~bernard/us3d.html
[2] Kremkau FW. Diagnostic ultrasound: principles and instruments. New York: Saunders; 2003.
[3] Tuthill T, Krucker J, Fowlkes J, Carson P. Automated three-dimensional US frame positioning computed from elevational speckle decorrelation. Radiology 1998;209(2):575–82.

[4] Detmer P, Bashein G, Hodges T, Beach K, Filer E, Burns D, Strandness D. 3D ultrasonic image feature localization based on magnetic scanhead tracking: in vitro calibration and validation. Ultrasound Med Biol 1994;20(2):923–36.

[5] Gobbi D, Comeau R, Peters T. Ultrasound probe tracking for real-time ultrasound/MRI overly and visualization of brain shift. Presented at medical image computing and computer-assisted intervention–MIMCCAI'99, Berlin, Germany 1999.

[6] King D, King DJ, Shao M. Three-dimensional spatial registration and interactive display of position and orientation of real-time ultrasound images. J Ultrasound Med 1990;9(9):525–32.

[7] http://mi.eng.cam.ac.uk/research/Biomed_Eng/cam_3dus.html

[8] Hossack JA, Sumanaweera TS, Ha JS. Quantitative 3D diagnostic ultrasound imaging using a modified transducer array and an automatted image tracking technique. IEEE Trans Ultrason Ferroelectr Freq Control 2002;49(8):1029–38.

[9] http://www.ljbdev.com/speckle.html

[10] Czerwinski RN, Jones DL, O'Brien WD. Ultrasound speckle reduction by directional median filtering. Proceeding of international conference on image process, vol. 1 1995 pp. 358–361.

[11] Hokland JH, Taxt T. Ultrasound speckle reduction using harmonic oscillator models. IEEE Trans on Ultrason Ferroelectr Freq Control 1994;41(2):215–24.

[12] Yu Y, Acton S. Speckle reducing anisotropic diffusion. IEEE Trans Image Process 2002;11(11):1260–70.

[13] Yu, Y. Ultrasound image enhancement for detection of contours using speckle reducing anisotropic diffusion, PhD dissertation; May 2003.

[14] Lee JS. Digital image enhancement and noise filtering by using local statistics. IEEE Trans Pattern Anal Machine Intell 1980;PAMI-2: 165–8.

[15] Frost VS, Stiles JA, Shanmugan KS, Holtzman JC. A model for radar images and its application to adaptive digital filtering of multiplicative noise. IEEE Trans Pattern Anal Machine Intell 1982; PAMI-4:157–65.

[16] Scherrer-Gosbie M, Steudel W, Hunziker PR, Foster GP, Garrido L, Liel-Cohen N, Zapol WM, Picard MH. Determination of Right Ventricular Structure and Function in Normoxic and Hypoxic Mice: a Transesophageal Echocardiographic Study. Circulation 1998;98: 1015–21.

[17] Dawson D, Lygate CA, Saunders J, Schneider JE, Ye X, Hulbert K, Noble JA, Neubauer S. Quantitative 3-Dimensional Echocardiography for Accurate and Rapid Cardiac Phenotype Characterization in Mice. Circulation 2004;110:1632–7.

[18] Bambre JC, Dickinson RJ. Ultrasonic B-scanning: a computer simulation. Phys Med Biol 1980;25(3):463–79.

[19] Pratt WK. Digital image processing. New York: Wiley; 1978. pp. 495–501.

[20] Canny A. Computational approach to edge detection. IEEE Trans Pattern Anal Machine Intell 1986;8(6):679–98.

[21] Yu Y, Acton ST. Three-dimensional speckle reducing anisotropic diffusion. Proceedings of the 37th asilomar conference on signals, systems and computers; 2003.

[22] http://143.129.203.3/visielab/sijbers/filter.html

Qingling Sun was born in Harbin, Hei Longjiang, China. She received her Master degree in computer Science from the Department of Computer Science in University of Virginia in 2004. Now she is working in Trionix, Inc. located in Ohio. Her research interests are 3D medical image processing, visualization of 3D medical imaging, and image enhancement for medical applications.

John A. Hossack was born in Glasgow, Scotland. He earned his B. Eng. Hons(I) in Electrical Electronic Engineering from Strathclyde University, Glasgow in 1986 and his PhD in the same department in 1990. From 1990 to 1992, Dr Hossack was a post doctoral researcher in the E. L. Ginzton Laboratory of Stanford University working under Prof B. A. Auld's guidance. His research was on modeling of 0:3 and 1:3 piezoelectric composite transducers. In 1992, he joined Acuson, Mountain View, CA initially working on transducer design. During his time at Acuson his interests diversified into beamforming and 3D imaging. Dr Hossack was made a Fellow of Acuson for 'excellence in technical contribution' in 1999. In 2000 he joined the Biomedical Engineering Department at the University of Virginia, Charlottesville, VA. His current interests are in improved 3D ultrasound imaging and high bandwidth transducers/signal processing with applications in cancer diagnosis and small animal imaging. Dr Hossack is a member of the IEEE and serves on both the Administrative Committee and the Technical Program Committee of the Ultrasonics section.

Jinshan Tang received his PhD degree from Beijing University of Posts and Telecommunications, P.R. China, in 1998. From September 1998 to June 2000, he worked as an invited researcher in ATR Media Integration and Communications Research Laboratories (MIC), Kyoto, Japan. In June 2000, he went to Harvard Medical School to work on image enhancement technology. Since Dec. 2001, Dr Tang has been working as a research scientist in Department of Electrical and Computer Engineering, University of Virginia. His research interests are medical image analysis, anisotropic diffusion, smart computers, content based image retrieval, active contour model, face detection and recognition, image enhancement for low-vision. Dr Jinshan Tang is a senior member of IEEE.

Scott T. Acton received the MS degree in Electrical and Computer Engineering and the PhD degree in Electrical and Computer Engineering from the University of Texas at Austin in 1990 and 1993, respectively, where he was a Microelectronics and Computer Development Fellow. He received the BS degree in Electrical Engineering from Virginia Tech, Blacksburg in 1988 as a Virginia Scholar. He has worked in industry for AT&T, Oakton, Va., the MITRE Corporation, McLean, Va. and Motorola, Inc., Phoenix, Az. and in academia for Oklahoma State University, Stillwater. For his research in video tracking, Dr Acton was given an ARO Young Investigator Award. He received the Halliburton Outstanding Young Faculty Award in 1998. In 1997, he was named the Eta Kappa Nu Outstanding Young Electrical Engineer—a national award that has been given annually since 1936. At the University of Virginia, Charlottesville, he was named the Outstanding New Teacher in 2002, elected a Faculty Fellow in 2003, and holds the Walter N. Munster chair in Electrical and Computer Engineering and Biomedical Engineering. He is the recipient of a Whitaker Foundation Biomedical Engineering Research Grant for work in cell detection and tracking. Dr Acton is an active participant in the IEEE, served as Associate Editor for the *IEEE Transactions on Image Processing* and as Associate Editor the *IEEE Signal Processing Letters*. He is the 2004 Technical Program Chair for the 38th *Asilomar Conference on Signals, Systems and Computers*. His research interests include anisotropic diffusion, active contours, biomedical segmentation problems, biomedical tracking problems and war.